Journal of Sound and Vibration 329 (2010) 1823–1835

Contents lists available at ScienceDirect

Journal of Sound and Vibration

journal homepage: www.elsevier.com/locate/jsvi

On the response of a harmonically excited two degree-of-freedom system consisting of a linear and a nonlinear quasi-zero stiffness oscillator

Gianluca Gatti [a,*], Ivana Kovacic [b], Michael J. Brennan [c]

[a] Department of Mechanical Engineering, University of Calabria, Arcavacata di Rende (CS) 87036, Italy
[b] Department of Mechanics, Faculty of Technical Sciences, University of Novi Sad, 21125 Novi Sad, Serbia
[c] Institute of Sound and Vibration Research, University of Southampton, Southampton SO17 1BJ, UK

ARTICLE INFO

Article history:
Received 17 July 2009
Received in revised form
9 November 2009
Accepted 13 November 2009
Handling Editor: M.P. Cartmell
Available online 31 December 2009

ABSTRACT

There are many systems which consist of a nonlinear oscillator attached to a linear system, examples of which are nonlinear vibration absorbers, or nonlinear systems under test using shakers excited harmonically with a constant force. This paper presents a study of the dynamic behaviour of a specific two degree-of-freedom system representing such a system, in which the nonlinear system does not affect the vibration of the forced linear system. The nonlinearity of the attachment is derived from a geometric configuration consisting of a mass suspended on two springs which are adjusted to achieve a quasi-zero stiffness characteristic with pure cubic nonlinearity. The response of the system at the frequency of excitation is found analytically by applying the method of averaging. The effects of the system parameters on the frequency-amplitude response of the relative motion are examined. It is found that closed detached resonance curves lying outside or inside the continuous path of the main resonance curve can appear as a part of the overall amplitude-frequency response. Two typical situations for the creation of the detached resonance curve inside the main resonance curve, which are dependent on the damping in the nonlinear oscillator, are discussed.

1. Introduction

Vibrating systems with purely nonlinear attachments have recently been the subject of growing interest of researchers. To a great extent, the studies have been inspired either by their interesting dynamics in *free* vibrating systems, fundamental aspects of which, including an energy transfer are reviewed in [1], or by their practical application where the nonlinear attachment acts as a passive sink for vibration attenuation of *forced* linear structures [2–8]. In such cases, the attached nonlinear system has a profound effect on the motion of the host structure, i.e., it acts as a nonlinear vibration absorber.

The nonlinearity in the system attached to a *forced* linear structure causes the coexistence of distinct new regimes, including periodic steady states and quasi-periodic response [3–6,8]. A distinctive feature of the multi-valuedness of the steady-state periodic response has been found for some values of the system parameters—a closed detached resonance curve occurring above the main continuous resonance curve [2,6,9]. In [2], the co-existence of high-amplitude localized

* Corresponding author. Tel.: +39 984 494157; fax: +39 984 494673.
E-mail address: g.gatti@unical.it (G. Gatti).

0022-460X/$ - see front matter © 2009 Elsevier Ltd. All rights reserved.
doi:10.1016/j.jsv.2009.11.019

solutions and low-amplitude solution over the same frequency range was predicted by applying the complexification-averaging method and it was verified experimentally. This feature is also found in [6] by applying the averaging method as well as by carrying numerical simulations to confirm it. In addition, a novel approach was developed therein, providing a sufficient condition for the occurrence of quasi-periodic response referred to as 'strongly modulated response', which is characterized by very deep oscillations of the modulated amplitude comparable to the amplitude of the response itself. An extensive numerical study of periodic responses of a nonlinear tuned mass damper was performed by using the numerical continuation software AUTO [9] and a family of detached parts of the frequency-resonance curves was discovered. Its appearance can be undesirable, because it may lead to vibrations of the host which are much higher than that of the main resonance curve. However, it was demonstrated in [7] that a properly tuned piecewise-quadratic damping element connecting a linear and a nonlinear oscillator, leads to complete elimination of this undesirable periodic response.

This study concerns a system in which the nonlinear attachment does not affect the response of the forced linear system and is not, therefore, concerned with nonlinear vibration absorbers. It follows on from the work presented in [10] by the authors. Therein, the dynamic behaviour of a nonlinear hardening single degree-of-freedom (SDOF) system attached to an electro-dynamic shaker, modelled as a harmonically excited linear SDOF system, was investigated. This was motivated by an experimental study, in which the force driving the shaker was kept constant with increasing frequency, and thus there was a strong shaker resonance in the frequency range of interest. Of particular interest was the situation when the linear natural frequency of the nonlinear system was less than the natural frequency of the shaker. It was found that although the shaker exhibited linear-like response, for some values of the system parameters, completely different shapes of the frequency-response curves (FRCs) for the nonlinear attachment could occur. It was observed that closed detached curves could appear outside or inside the main resonance curve, and a physical explanation for their occurrence was given. Such a system could, for example, be a nonlinear isolator under test. There are significant advantages in adjusting the nonlinearity of an isolator so that it has a quasi-zero stiffness (QZS) characteristic [11,12], which motivates the need for the analysis of such a system attached to a linear system (the shaker) in which the behaviour of the nonlinear system, again, does not affect the response of the linear system.

In this paper such a system is considered. The frequency-response curves corresponding to the steady-state response of the nonlinear system at the frequency of excitation are studied. The appearance of an outer or inner detached curve is found here, too. Attention is focused on the way in which the shape of the FRCs changes, and how the detached curves are formed. The occurrence of the inner part of the FRC, named after its shape, a *bubble*, is of interest as it can yield a response where the amplitude is lower than that of the main resonance curve. This distinguishable characteristic of the QZS system attached to the linear oscillator has not been observed in previous studies of similar systems [2–8].

This paper is organized as follows. Section 2 contains a mechanical and mathematical model of the system considered with a description of how a QZS characteristic is achieved. In addition, in this section the corresponding steady-state solutions are given. In Section 3, the effects of the system parameters on the characteristics of the FRCs are considered both analytically and numerically. In particular, the role of damping in the creation of the detached resonance curve is discussed. In Section 4, some approximate analytical expressions are derived which can be used to determine the shape of the FRCs. Section 5 contains conclusions.

2. Model of the system and amplitude-frequency equations

The configuration of the nonlinear system, which is attached to the linear oscillator, considered in this paper is shown in Fig. 1a. The mass m is connected by two springs to the linear oscillator by a support structure. It vibrates in the horizontal direction causing the springs to incline, creating geometric nonlinearity. The corresponding force f—deflection z relationship is given by

$$f = 2kz\left(1-\frac{d_0}{\sqrt{z^2+d^2}}\right), \tag{1}$$

where d_0 is the length of the unstretched springs and d is equal to the length of the spring when the system is at rest, i.e. when the springs are vertical. Using the Maclaurin-series expansion to the third order for small z, Eq. (1) results in

$$f \approx k_1 z + k_3 z^3, \tag{2}$$

where $k_1 = 2k(1-d_0/d)$ and $k_3 = k(d_0/d^3)$. To adjust the system so that it has a quasi-zero stiffness characteristic, k_1 should be set to zero. This implies that the springs must be neither stretched nor compressed at rest, that is $d_0/d = 1$. A non-dimensional form of Eq. (1) and its approximation given by Eq. (2) are illustrated in Fig. 1b, for $k_1 = 0$. It can be seen that for displacements $z < 40$ percent of the length d, the percentage error between Eqs. (1) and (2) is < 5 percent.

The small mass m is attached with the QZS spring configuration to a linear oscillator which has a much larger moving mass m_s. The linear oscillator is modelled as a parallel combination of the mass m_s, linear spring k_s and damper c_s excited by a harmonic force $F\cos(\omega t)$ [10], with a constant amplitude. A model of these coupled systems is shown in Fig. 2. Such a configuration may be realized, for example, by attaching the nonlinear system to an electro-dynamic shaker [10].

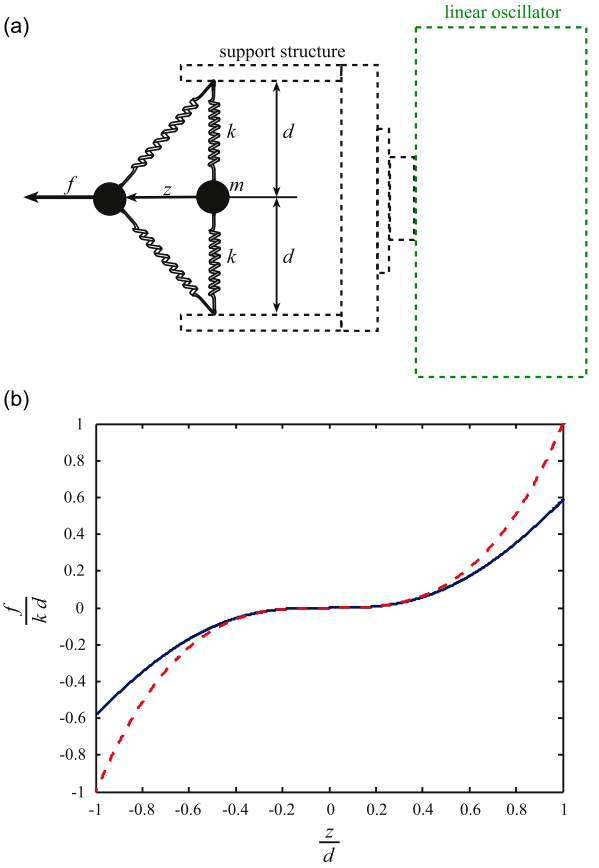

Fig. 1. Geometric nonlinearity due to the springs arrangement: (a) schematic view, and (b) reaction force as a function the mass displacement in non-dimensional form for a QZS case; exact expression given by Eq. (1) (blue solid line) and approximate expression given by Eq. (2) (red dashed line). (For interpretation of the references to the colour in this figure legend, the reader is referred to the web version of this article.)

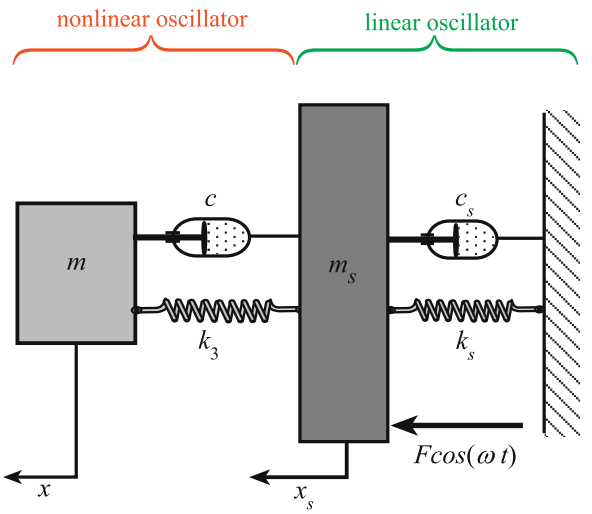

Fig. 2. Schematic view of the 2-DOF system under consideration.

Using the approximate expression for the spring restoring force given by Eq. (2) with $k_1 = 0$, the equations of motion of this two degree-of-freedom (2-DOF) system are given by

$$m_s\ddot{x}_s + c_s\dot{x}_s + k_s x_s + c(\dot{x}_s - \dot{x}) + k_3(x_s - x)^3 = F\cos(\omega t), \quad m\ddot{x} - c(\dot{x}_s - \dot{x}) - k_3(x_s - x)^3 = 0. \tag{3a,b}$$

Noting that $z = x_s - x$, and introducing the non-dimensional variables

$$y_s = \frac{x_s}{x_0}, \quad y = \frac{x}{x_0}, \quad w = \frac{z}{x_0}, \quad x_0 = F/k_s, \quad \omega_s = \sqrt{k_s/m_s}, \quad \tau = \omega_s t, \quad \Omega = \frac{\omega}{\omega_s}, \quad \mu = \frac{m}{m_s}, \quad \gamma = \frac{k_3}{\mu k_s} x_0^2, \quad \zeta_s = \frac{c_s}{2m_s\omega_s}, \quad \zeta = \frac{c}{2m\omega_s}, \tag{4a-l}$$

Eqs. (3a,b) can be expressed in non-dimensional form as

$$(w'' + y'') + 2\zeta_s(w' + y') + (w + y) + 2\mu\zeta w' + \mu\gamma w^3 = \cos(\Omega\tau), \quad y'' - 2\zeta w' - \gamma w^3 = 0, \tag{5a,b}$$

where primes denote differentiation with respect to non-dimensional time τ. It should be noted that a change in γ can be interpreted as a change in the nonlinearity or in the amplitude of excitation or in the mass ratio. It is also noted that x_0, as defined by Eq. (4d), represents the static displacement at $\omega = 0$.

Summing up Eqs. (5a,b) and assuming that $|\mu\ddot{y}| \ll |\ddot{y}_s|$, yields

$$y_s'' + 2\zeta_s y_s' + y_s = \cos(\Omega\tau), \quad w'' + 2\zeta w' + \gamma w^3 = y_s'' . \tag{6a,b}$$

Eq. (6a) indicates that the nonlinear system has a negligible effect on the vibration of the large mass, so that it vibrates as a linear system. Eq. (6b) describes a base-excited hardening Duffing oscillator with no linear stiffness term.

2.1. Amplitude-frequency equations

Of interest in this paper is to find the response at the frequency of excitation. The corresponding steady-state harmonic oscillation resulting from Eq. (6a) is [13]

$$y_s = Y_s \cos(\Omega\tau + \varphi_s), \tag{7}$$

in which the amplitude is given by

$$Y_s = \sqrt{\frac{1}{(1-\Omega^2)^2 + 4\zeta_s^2\Omega^2}}. \tag{8}$$

Applying the method of averaging of the first order [13], the stationary response at the frequency of excitation is found to be

$$w = W \cos(\Omega\tau + \varphi), \tag{9}$$

where the steady-state amplitude of the relative displacement W satisfies

$$\tfrac{9}{16}\gamma^2 W^6 - \tfrac{3}{2}\gamma\Omega^2 W^4 + (\Omega^4 + 4\zeta^2\Omega^2)W^2 - \Omega^4 Y_s^2 = 0. \tag{10}$$

It should be noted that Eq. (10) is coupled with Eq. (8) by the amplitude of the response Y_s. The focus of this paper is on the amplitude-frequency relationships, so the expressions for the phases φ_s and φ are not given.

The stability of the steady-state solution was calculated following the procedure in [14] and the limits for stability were determined to be

$$\Omega_{1,2} = \sqrt{\left(\frac{3}{2}W^2\gamma - 2\zeta^2\right) \pm \sqrt{\left(-\frac{3}{2}W^2\gamma + 2\zeta^2\right)^2 - \frac{27}{16}W^4\gamma^2}}. \tag{11}$$

In the FRCs plotted in this paper the stable solutions are depicted by solid lines and unstable solutions by dashed lines.

By numerical integration of Eqs. (5a,b) with the mass ratio fixed to $\mu = 0.001$ to satisfy the assumption $|\mu\ddot{y}| \ll |\ddot{y}_s|$, it was verified that the response of the system is periodic at the frequency of excitation, and higher harmonics are negligible. Numerical results are presented in the following section.

3. Effects of system parameters

In this section, the effects of the nonlinear parameter γ, the damping ratio of the linear system ζ_s, and the damping ratio of the nonlinear oscillator ζ on the shape of the FRCs of the relative displacement amplitude W are investigated. The FRCs of the displacement amplitude Y_s are not shown; however, it should be noted that Eqs. (5a,b) were integrated numerically to confirm that the response of the large mass was predominantly cosinusoidal i.e. Eqs. (7) and (8) were satisfied.

Due to the nonlinearity in the system, there are combinations of the parameters which yield a multi-valued response. To find the conditions for such response, the amplitude-frequency Eq. (10) is treated as a cubic in W^2. Depending whether its discriminant is negative or positive, Eq. (10) can have one or three distinct real roots, respectively. The transition between these two cases is determined by setting the discriminant to zero to give

$$\gamma_{1,2} = \frac{8}{81\Omega}\left[36\zeta^2\Omega + \Omega^3 \pm (\Omega^2 - 12\zeta^2)^{3/2}\right]\left[(\Omega^2-1)^2 + 4\zeta_s^2\Omega^2\right], \tag{12a,b}$$

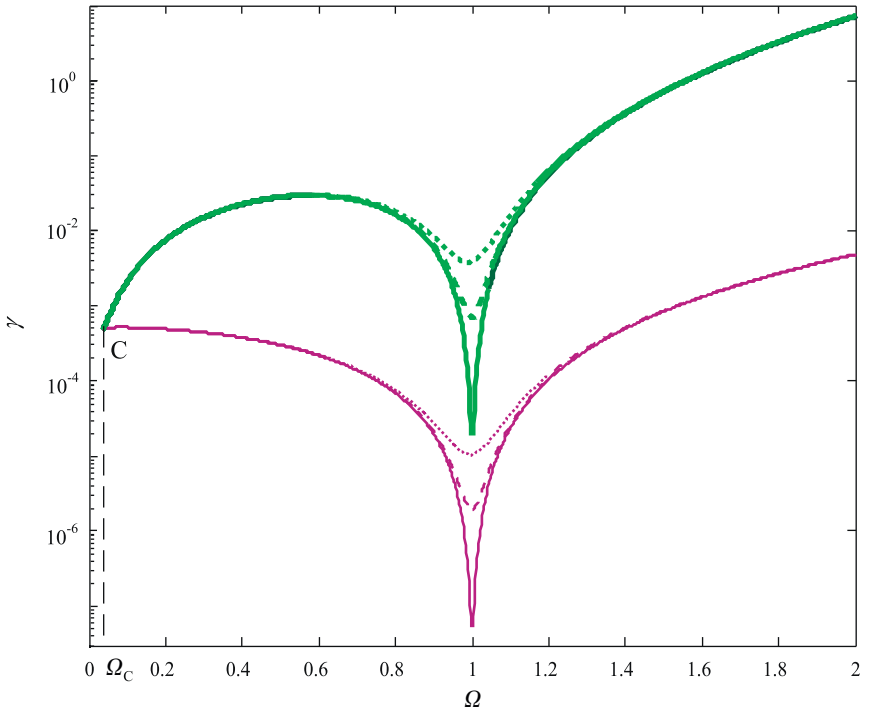

Fig. 3. Effects of the damping parameter ζ_s on the bifurcation curves given by Eq. (12a), depicted by a thick line and Eq. (12b), depicted by a thin line, defining the transition from one to three real solutions for the frequency-amplitude response of W, for $\zeta = 0.03$: $\zeta_s = 0.005$ (solid curve); $\zeta_s = 0.03$ (dash curve); and $\zeta_s = 0.07$ (dot curve).

For values of nonlinearity between γ_1 and γ_2 any combination of the parameters ζ_s, ζ and Ω yields three distinct real solutions for the amplitude W. Eqs. (12a,b) are used to plot the bifurcation curves in the $\Omega-\gamma$ plane in Figs. 3 and 4, in which the effects of the damping in the linear and nonlinear oscillators are illustrated. In particular, in Fig. 3 these curves are shown for a fixed value of $\zeta = 0.03$ and for several values of ζ_s. It can be seen that a change in the value of ζ_s has the same effect on γ_1 and γ_2, i.e. only shifting the position of the local minima of these curves, which occur approximately at $\Omega \approx 1$. In Fig. 4 and movie1, these curves are shown for a fixed value of $\zeta_s = 0.03$ and for different values of ζ. They illustrate that the damping in the attached system has a different effect on γ_1 and γ_2 . It should be noted that, depending on the value of ζ, the upper curve can have a maximum of three extrema points, while the lower curve can have up to two extrema points, the importance of which is discussed in the following subsection. The relative minima of both curves occur at $\Omega \approx 1$, but only the one on the upper curve is slightly affected by ζ. Also, the relative maximum of the upper curve and the corresponding frequency, $\Omega \approx 1/\sqrt{3}$, appear not to be affected either.

The upper and lower curves intersect at point C, whose position can be determined by setting $\gamma_1 = \gamma_2$, to give

$$(\Omega_C, \gamma_C) = \left(2\sqrt{3}\zeta, \tfrac{128}{27}\zeta^2[(1-12\zeta^2)^2 + 48\zeta^2\zeta_s^2]\right). \tag{13}$$

It should be observed from Figs. 3 and 4, where this point is shown, that the bifurcation boundaries, i.e. the multi-valued response, only exist at frequencies greater than Ω_C. This frequency increases linearly with ζ and does not depend on ζ_s. The intersection point C is important since the bifurcation curves are not defined for frequencies lower than Ω_C. Thus, if Ω_C is greater than unity, which occurs when $\zeta \approx 1/2\sqrt{3}$, no local maxima or minima exist. In the special case when $\zeta = 0$, Eqs. (12a,b) reduces to

$$\gamma_1 = \gamma_2 = \tfrac{16}{81}\left[\Omega^2(\Omega^2-1)^2 + 4\Omega^4\zeta_s^2\right], \tag{14}$$

which results in a single bifurcation curve in the $\Omega-\gamma$ plane. For the combination of parameters below this curve, depicted by the solid line in Fig. 4, three distinct real roots of Eq. (10) exist. In this case point C coincides with the origin, and a multi-valued response occurs for any value of frequency.

3.1. Characteristic regions in the $\Omega-\gamma$ plane and corresponding FRCs

Depending on the values of the system parameters, several different shapes of the FRC of W can be identified. To help to categorize these shapes, the local maxima on the lower and the upper bifurcation curve are labelled T_1 and

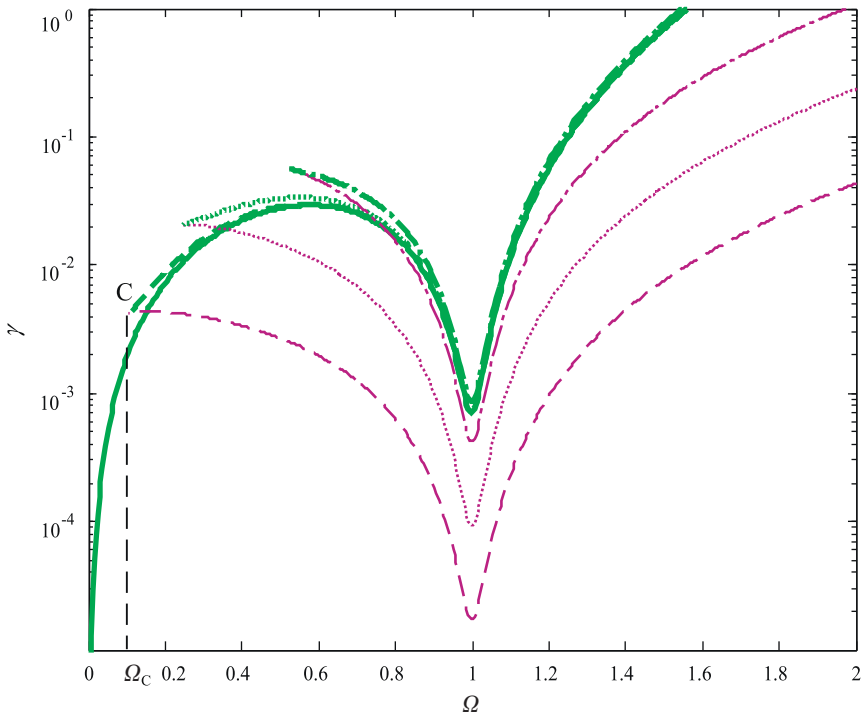

Fig. 4. Effects of the damping parameter ζ on the bifurcation curves given by Eq. (12a), depicted by a thick line and Eq. (12b), depicted by a thin line, defining the transition from one to three real solutions for the frequency-amplitude response of W, for $\zeta_s = 0.03$: $\zeta = 0$ (solid curve); $\zeta = 0.03$ (dash curve); $\zeta = 0.07$ (dot curve); $\zeta = 0.15$ (dash-dot curve).

T_2, respectively, while the local minima on the upper and the lower curve are labelled T_3 and T_4, respectively. These points together with point C are calculated numerically from Eqs. (12a,b) and (13), and are used to define regions which characterize the different shapes of the FRCs. These are shown in Figs. 5a and b for two different combinations of ζ and ζ_s. Although Figs. 5a and b appear to be similar, they are different with respect to the positions of points T_1 and T_3. Thus, the characteristic regions are presented as regions I, II, IIIa, IV and V in Fig. 5a, and as regions I, II, IIIb, IV and V in Fig. 5b. These two cases illustrate typical ways in which the FRCs change with the system parameters.

The shapes of the FRCs that correspond to each of the regions shown in Fig. 5a are illustrated in Figs. 6a–f. The stable and unstable parts of the FRCs are indicated by solid and dashed lines, respectively. In Fig. 6a, which corresponds to region I, where the nonlinear parameter is very small, it can be seen that the FRC is single-valued and similar to that of a linear system. For higher values of γ, corresponding to region II, a closed *detached resonance curve* appears above the main FRC around $\Omega \approx 1$, with a stable and an unstable part as shown in Fig. 6b. As γ is further increased, the detached resonance curve enlarges and approaches the main FRC. The detached resonance curve joins it at its peak, at a frequency of $\Omega \approx 1$, as shown in Fig. 6c, which corresponds to region IIIa. Increasing the value of γ even further, a closed detached resonance curve is formed, lying inside the main resonance curve as shown in Fig. 6d, corresponding to region IV. This detached curve is named after its shape—a *bubble* [10], and it also has a stable and an unstable part. As γ is further increased within region IV, the bubble becomes smaller and smaller as illustrated in Fig. 6e before it disappears. This corresponds to the boundary between regions IV and V. The FRC depicted in Fig. 6f corresponds to region V.

To validate the approximate analytical solutions for the parameters used to plot Figs. 6a–f, Eqs. (5a,b) were solved numerically and the Fourier coefficients were extracted from the time histories. The first of these coefficients is depicted in Figs. 6a–f as circles. Moreover, it was verified that, for the parameters used in this work, the amplitudes of the higher harmonics were negligible compared to the fundamental. To further illustrate the effect of γ, movie2 shows the way in which the shapes of the FRCs change as γ increases.

Figs. 7a–f illustrate the way in which the FRCs change when the regions in Fig. 5b exist. The distinguishable feature in this case is the way in which the bubble is created. The outer detached resonance curve merges with the main resonance curve at a lower frequency $\Omega \approx 0$, as shown in Fig. 7c. Then its unstable part and the peak of the main resonance curve occurring at $\Omega \approx 1$ coalesce, forming a bubble as shown in Fig. 7d. By increasing γ further, the bubble reduces in size as shown in Fig. 7e and disappears as in the previous case. The numerically obtained results are again presented as circles in Figs. 7a–f. The movie (movie3) further illustrates the behaviour as γ is increased.

To emphasize the relationship between the bifurcation curves in the $\Omega-\gamma$ plane and the FRCs in the $\Omega-W$ plane, a three-dimensional graph involving the three variables Ω, γ, W is plotted in Fig. 8. Two graphs are shown (Figs. 8a and b) to illustrate the relationship between the bifurcation curves in Fig. 5a and the FRCs of Figs. 6b and d. It can be seen that a

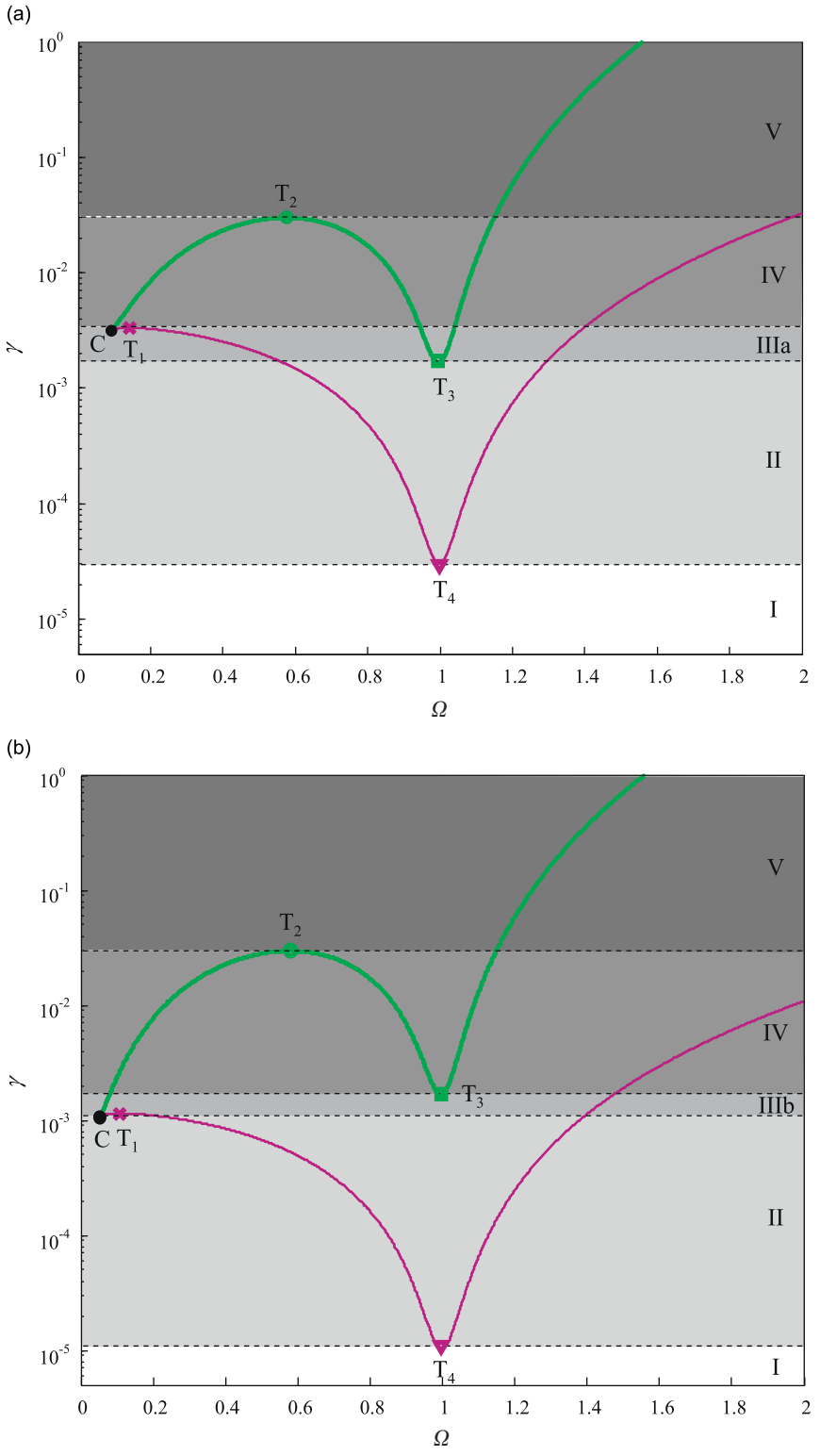

Fig. 5. Characteristic regions I–V in the Ω-γ plane, where the FRC of W exhibits different shapes, for $\zeta_s = 0.046$: (a) $\zeta = 0.026$; (b) $\zeta = 0.015$. Characteristic points T_1, T_2, T_3, T_4 and C are also labelled.

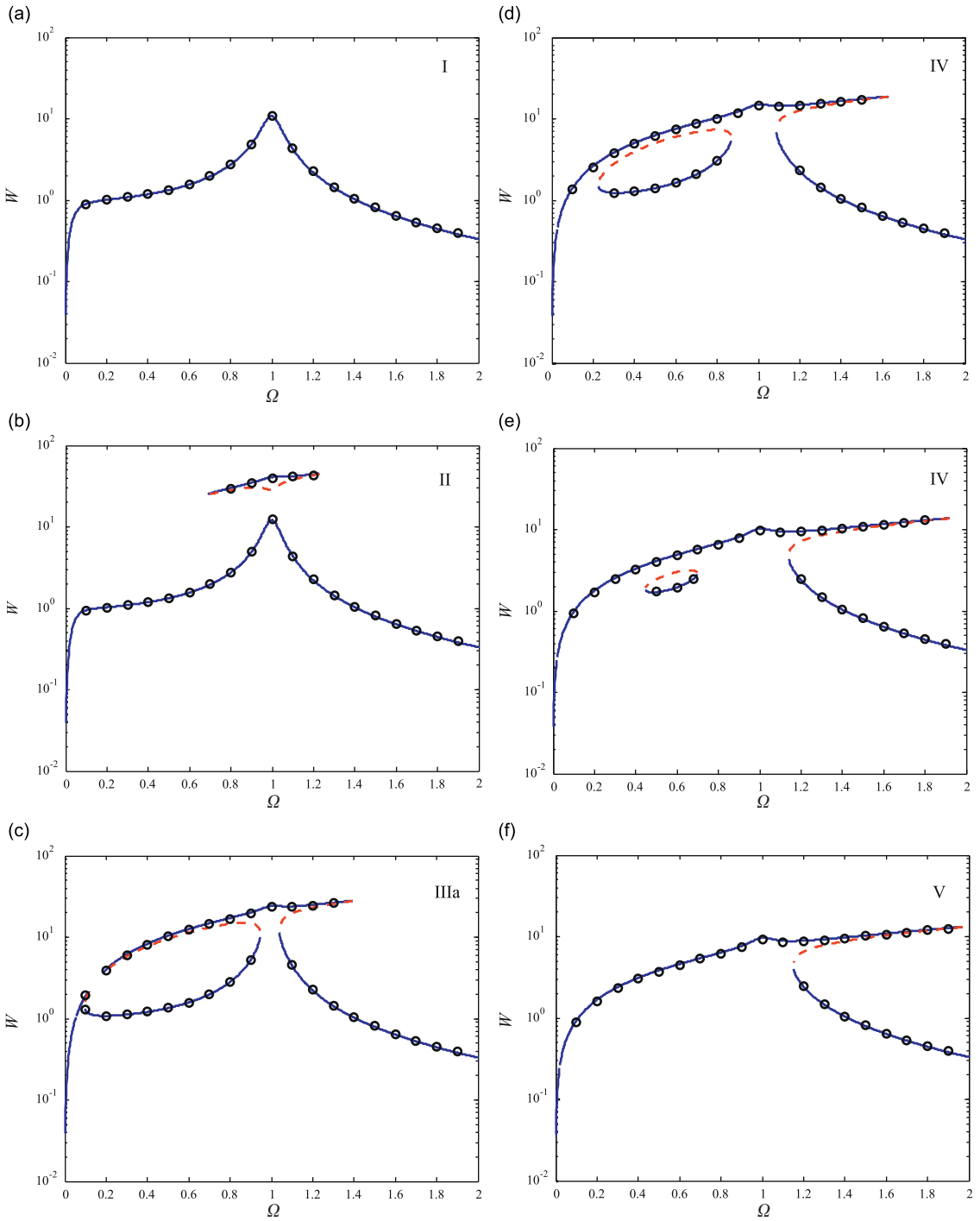

Fig. 6. FRCs of the normalized relative displacement W as a function of the normalized frequency Ω for $\zeta_s = 0.046$, $\zeta = 0.026$ and for different values of the nonlinear parameter γ: (a) $\gamma = 10^{-5}$; (b) $\gamma = 10^{-3}$; (c) $\gamma = 3.3 \times 10^{-3}$; (d) $\gamma = 10^{-2}$; (e) $\gamma = 2.6 \times 10^{-2}$; and (f) $\gamma = 3 \times 10^{-2}$. Stable solution (blue solid line), unstable solution (red dashed line). Numerical solution by integrating Eqs. (5a, b) (black '○'). (For interpretation of the references to the colour in this figure legend, the reader is referred to the web version of this article.)

straight line, drawn for a particular value of γ, may be interpreted as the projection of the corresponding FRC on the $\Omega-\gamma$ plane. Moreover, the intersections between this straight line and the bifurcation curves give the values of the jump frequencies: the upper green bifurcation curve corresponding to jumps-up, and the lower magenta bifurcation curve corresponding to jumps-down.

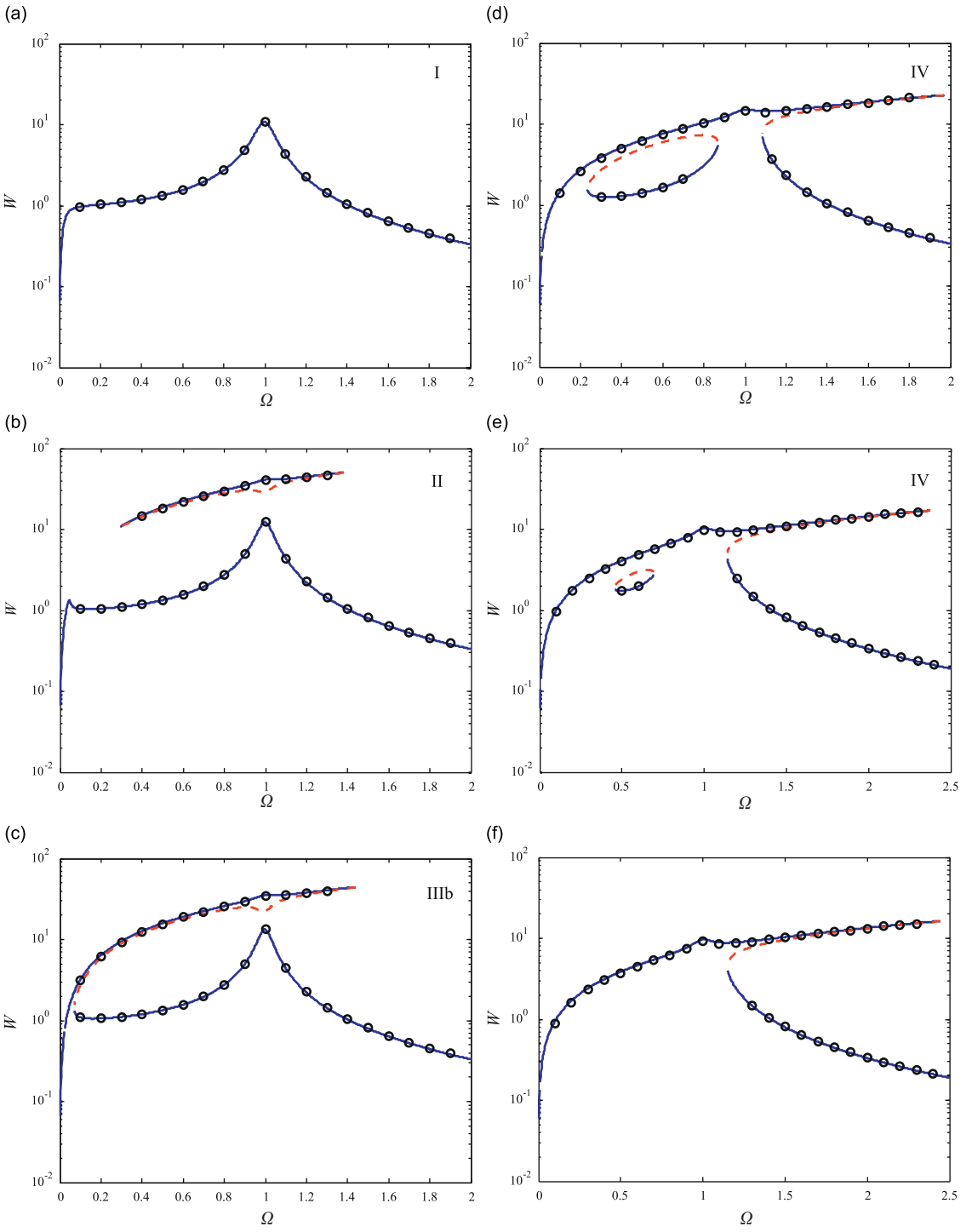

Fig. 7. FRCs of the normalized relative displacement W as a function of the normalized frequency Ω for $\zeta_s = 0.046$, $\zeta = 0.015$ and for different values of the nonlinear parameter γ: (a) $\gamma = 10^{-5}$; (b) $\gamma = 10^{-3}$; (c) $\gamma = 1.4 \times 10^{-3}$; (d) $\gamma = 10^{-2}$; (e) $\gamma = 2.6 \times 10^{-2}$; and (f) $\gamma = 3 \times 10^{-2}$. Stable solution (blue solid line), unstable solution (red dashed line). Numerical solution by integrating Eqs. (5a,b) (black '○'). (For interpretation of the references to the colour in this figure legend, the reader is referred to the web version of this article.)

3.2. *Characteristic regions in the $\zeta-\gamma$ plane*

Figs. 5a and b show the regions corresponding to particular shapes of the FRCs and the formation of the bubble. However, they were plotted for only two particular combinations of the damping parameters. To give more general insight

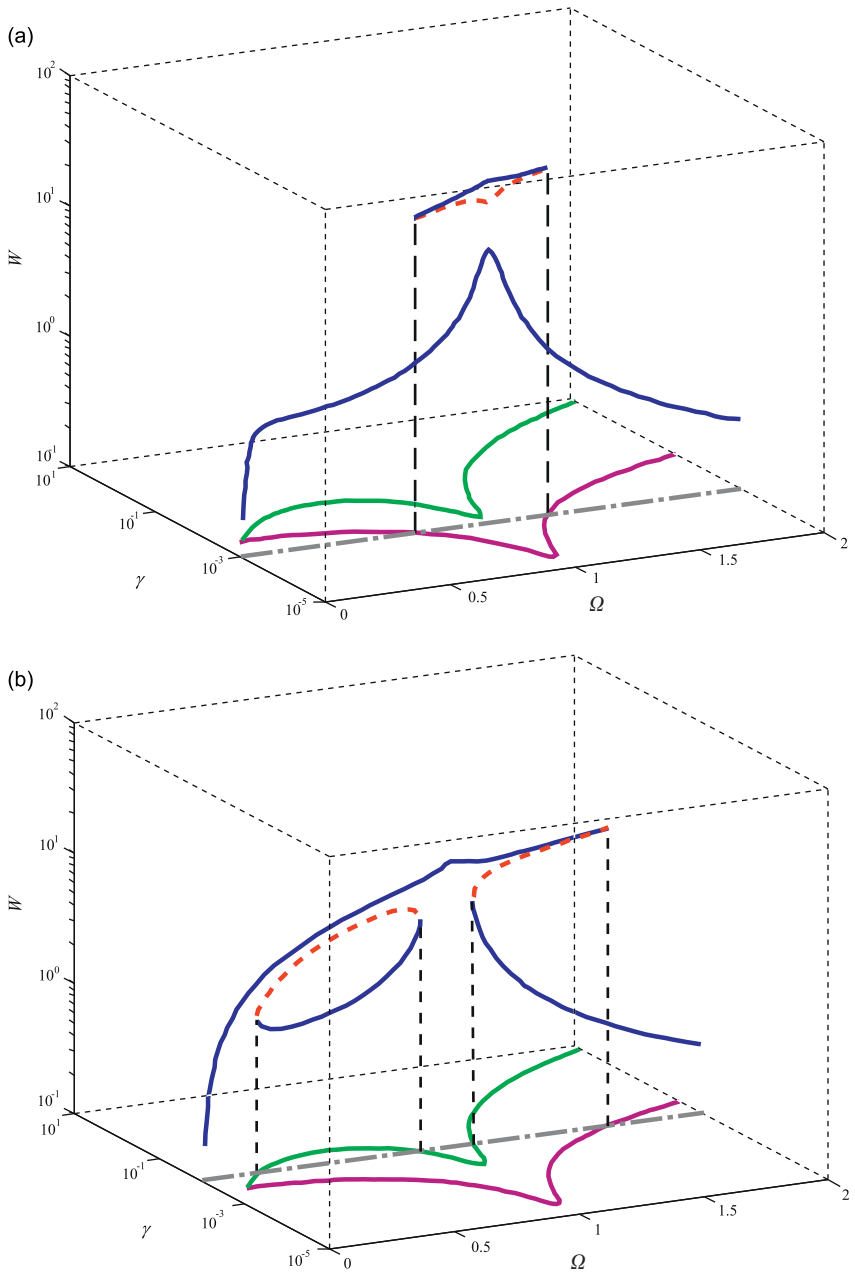

Fig. 8. Three-dimensional plot illustrating the relationship between the bifurcation curves in Fig. 5a, and the FRCs in: (a) Fig. 6b and (b) Fig. 6d.

into the influence of the parameters of the nonlinear attachment on these features, the characteristic regions can be identified in the $\zeta-\gamma$ plane. The boundaries of these regions are found by using the coordinates of the points T_1–T_4. They are obtained by differentiating Eqs. (12a,b) with respect to Ω, setting it to zero and solving it numerically for a specific value of damping in the linear oscillator, $\zeta_s = 0.046$. The values of γ corresponding to these points are then plotted in Fig. 9. The γ-coordinate of point C is also plotted as a function of ζ as defined by Eq. (13). The regions I, II, IIIa, IIIb, IV and V are also identified and shaded as in Fig. 5.

It can be seen from Fig. 9 that the γ values of point T_1 follow the same trend as point C, in a way that the corresponding curves are almost indistinguishable from each other. The curves corresponding to the location of points T_1 and T_2 seem to intersect with the curve of point C at point Q. For the case $\zeta > \zeta_Q$, the former two curves disappear, implying that the lower and the upper bifurcation curves in the $\Omega-\gamma$ plane do not have a local maximum any more. Similarly, it is seen from Fig. 9 that the points T_3 and T_4 do not exist for $\zeta > \zeta_R$, where point R represents the intersection with the curve for point C. Point P

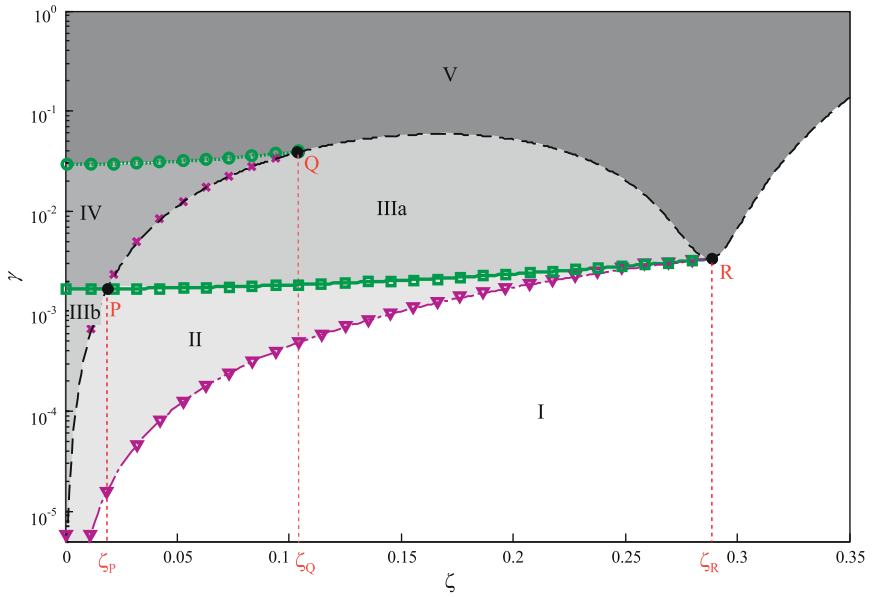

Fig. 9. Characteristic regions I–V in the ζ-γ plane, for $\zeta_s = 0.046$; point C from Eq. (13) (dash black line); numerical solution for the relative maximum T_2 (green '○') and minimum T_3 (green '□') of the upper bifurcation curve of Eq. (12a); numerical solution for the relative maximum T_1 (magenta '×') and minimum T_4 (magenta '∇') of the lower bifurcation curve of Eq. (12b); approximate solutions for the relative maximum T_2 given by Eq. (16) (thick green dotted line), minimum T_3 given by Eq. (17a) (thick green solid line) and minimum T_4 given by Eq. (17b) (thin magenta dashed-dotted line). The location of points P, Q and R, depicted by black dots, are defined by Eqs. (20), (18) and (19), respectively. (For interpretation of the references to the colour in this figure legend, the reader is referred to the web version of this article.)

is also labelled in Fig. 9, which coincides with the point where points T_3 and T_1, i.e. C are equal. Depending on the location of the characteristic points T_1–T_4 as well as P, Q and R, the plane $\zeta-\gamma$ can also be divided into characteristic regions, as presented in Fig. 9. Thus, if the damping ζ is fixed at a particular value and the nonlinearity γ is increased, several situations regarding the transformation of the FRCs can be distinguished. If $0<\zeta<\zeta_P$, the FRCs undergo the transformation I–II–IIIb–IV–V, as shown in Fig. 5b with the characteristic FRCs given in Fig. 7. When $\zeta_P<\zeta<\zeta_Q$, the FRCs change according to the regions I–II–IIIa–IV–V, with the characteristic FRCs plotted in Fig. 6. The transformations that occur for higher values can be considered as special cases of this one, with some of the regions and shapes omitted. If $\zeta_Q<\zeta<\zeta_R$, the path I–II–IIIa–V is followed, implying that the bubble, which is a main feature of the region IV, does not appear in the corresponding response. When $\zeta>\zeta_R$, the path I–V is followed, which means that neither the outer nor the inner detached curve occur.

One point should be noted regarding the above discussion. It regards the fact that the location of point T_1 and C have been treated as being coincident, and as a result no region was identified between them in Fig. 9. If it had been considered, it would have either belonged to regions II or IIIa. In this respect no new region is discarded by the approximation. What actually happens in such a narrow region is the appearance of a small tiny peak at a very low frequency in the FRC of W, which has both a stable and an unstable part (see Fig. 6c as an example). It means that 'small' jumps may also appear at lower frequencies for a very particular combination of the system parameters.

4. Approximate expressions for the points characterizing the shapes of the FRCs

The variables γ and ζ corresponding to the points that characterize the shapes of the FRCs shown in Fig. 9 can be determined approximately in an analytical form, provided that they are restricted to the range used to plot Fig. 9, and it is also assumed that $\zeta_s \ll 1$. It has been mentioned that the curve corresponding to point T_1 can be approximated by the one corresponding to point C. So, if the equation for point C given by Eq. (13) is used, one obtains

$$\gamma_{T_1} \approx \gamma_C \approx \frac{128}{27}\zeta^2(1-12\zeta^2)^2. \tag{15}$$

While considering the $\Omega-\gamma$ plane plotted in Figs. 3 and 4 (see the beginning of Section 3), it was observed that the value of Ω corresponding to T_2 was only slightly affected by the damping parameters ζ and ζ_s, and is given approximately by $\Omega = 1/\sqrt{3}$. Substituting this into Eq. (12a) results in

$$\gamma_{T_2} \approx \frac{32}{2187}\left[1+108\zeta^2+\sqrt{(1-36\zeta^2)^3}\right]. \tag{16}$$

In addition, $\Omega \approx 1$ for the points T_3 and T_4. Thus, substituting for $\Omega = 1$ into Eq. (12a,b) gives

$$\gamma_{T_3} \approx \frac{32}{81}\zeta_s^2\left[1+36\zeta^2+\sqrt{(1-12\zeta^2)^3}\right]$$

$$\gamma_{T_4} \approx \frac{32}{81}\zeta_s^2\left[1+36\zeta^2-\sqrt{(1-12\zeta^2)^3}\right]. \quad (17a,b)$$

To validate the approximate expressions of Eqs. (16) and (17), they are used to plot the location of points T_2, T_3 and T_4 in the plane $\zeta-\gamma$ in Fig. 9 as a thick green dotted line, a thick green solid line and a thin magenta dashed-dotted line, respectively. It can be seen that they almost coincide with the numerical solutions for these points, obtained by solving Eqs. (12a,b), which are depicted by green circles, green squares and magenta triangles, respectively.

It was also observed earlier (see Section 3.2 and Fig. 9) that the inner detached curve does not occur for $\zeta > \zeta_Q$. The system parameters yielding this case can be obtained by equating Eqs. (15) and (16) to give

$$(\zeta_Q, \gamma_Q) \approx (0.1036, 0.0386). \quad (18)$$

The intersection of the curves for T_3 and T_4 in Fig. 9 defines point R. Hence, equating Eqs. (17a) and (17b), one derives

$$(\zeta_R, \gamma_R) \approx \left(\frac{1}{2\sqrt{3}}, \frac{128}{81}\zeta_s^2\right). \quad (19)$$

Eqs. (18) and (19) define the minimum values of the damping ratio and the corresponding nonlinearity for which the detached curves do not appear in the amplitude-frequency diagrams: the bubble by Eq. (18) and none of the detached curves by Eq. (19).

A simple approximate expression for point P may be found as it occurs at the intersection of the curves for T_3 and C. It is observed that point T_3 is only slightly influenced by ζ, as evident from Figs. 4 and 9. Thus, the value of γ may be calculated by setting $\zeta = 0$ in Eq. (17a) to give $\gamma_P = \frac{64}{81}\zeta_s^2$. The corresponding value of ζ can be determined by substituting this into Eq. (13), for small ζ, to give

$$(\zeta_P, \gamma_P) \approx \left(\frac{\zeta_s}{\sqrt{6}}, \frac{64}{81}\zeta_s^2\right). \quad (20)$$

Thus the damping ratio for the nonlinear oscillator corresponding to point P is proportional to ζ_s.

This point defines the boundary between the two ways in which the detached curve merges with the main FRC. This is in contrast with the damping parameter ζ corresponding to points Q and R, which is independent of ζ_s. Eqs. (18)–(20) for the points Q, R and P are used to label their position in Fig. 9 by black dots. They imply that these approximate analytical expressions define their position well with respect to the intersection of the curves which create them.

5. Conclusions

In this paper, an investigation of a two degree-of-freedom forced nonlinear system has been presented. The system is representative of a QZS SDOF system being excited by a linear oscillator which has a much larger moving mass than the QZS system. Such a system would be representative of a nonlinear isolator having a QZS characteristic being excited by an electro-dynamic shaker with a constant current. The method of averaging has been applied to determine the amplitude-frequency equation of the relative motion of the smaller mass at the excitation frequency and the stability condition which defines stable and unstable steady-states solutions has been derived. The effects of the system parameters on this amplitude-frequency response have been investigated analytically and numerically. It has been found that the frequency-response curve can have several distinguishable shapes within the regions of multi-valued steady states. This multi-valuedness can be the consequence of the bending of the main continuous resonance curve or the occurrence of closed *detached resonance curves*. These detached curves can lie outside or inside the main resonance curve. The latter has a shape of a *bubble*. Two typical possibilities of how the bubble is created have been shown. In the region where the bubble exists, the system can have two stable steady-state solutions. It has also been shown that depending on the values of the system parameters several distinct shapes of the amplitude-frequency response can occur. The value of the damping ratio of the nonlinear attachment has been identified for which the bubble does not appear as well the one yielding the response without any outer/inner detached curve. Approximate analytical expressions that define the boundaries between the shapes of the frequency response have been determined allowing the parameters that influence the shape to be identified.

Acknowledgement

Professors Brennan and Kovacic would like to acknowledge the support received from the Royal Society, UK, International Joint Project ‘Using nonlinearity to improve the performance of vibrating systems’.

Appendix A. Supplementary material

Supplementary data associated with this article can be found in the online version at doi:10.1016/j.jsv.2009.11.019.

References

[1] Y.S. Lee, A.F. Vakakis, L.A. Bergman, D.M. McFarland, G. Kerschen, F. Nucera, P. Pangopoulos, S. Tzakirtzis, Passive nonlinear TET and its applications to vibration absorption: a review, *Journal of Multi-Body Dynamics (IMechE—Part K)* 222 (2008) 77–134.
[2] X. Jiang, M. McFarland, L.A. Bergman, A.F. Vakakis, Steady state passive nonlinear energy pumping in coupled oscillators: theoretical and experimental results, *Nonlinear Dynamics* 33 (2003) 7–102.
[3] O.V. Gendelman, E. Gurdon, C.H. Lamarque, Quasiperiodic energy pumping in coupled oscillators under periodic forcing, *Journal of Sound and Vibration* 294 (2006) 651–662.
[4] O.V. Gendelman, Y. Starosvetsky, M. Feldman, Attractors of harmonically forced linear oscillator with attached nonlinear energy sink I: description of response regimes, *Nonlinear Dynamics* 51 (2008) 31–46.
[5] Y. Starosvetsky, O.V. Gendelman, Attractors of harmonically forced linear oscillator with attached nonlinear energy sink. II: optimization of a nonlinear vibration absorber, *Nonlinear Dynamics* 51 (2008) 47–57.
[6] Y. Starosvetsky, O.V. Gendelman, Response regimes of linear oscillator coupled to nonlinear energy sink with harmonic forcing and frequency detuning, *Journal of Sound and Vibration* 315 (2008) 746–765.
[7] Y. Starosvetsky, O.V. Gendelman, Vibration absorption in systems with a nonlinear energy sink: nonlinear damping, *Journal of Sound and Vibration* 324 (2009) 916–939.
[8] E. Gourdon, N.A. Alexander, C.A. Taylor, C.H. Lamarque, S. Pernot, Nonlinear energy pumping under transient forcing with strongly nonlinear coupling: theoretical and experimental results, *Journal of Sound and Vibration* 300 (2007) 522–551.
[9] N.A. Alexander, F. Schilder, Exploring the performance of a nonlinear tuned mass damper, *Journal of Sound and Vibration* 319 (2009) 445–462.
[10] G. Gatti, M.J. Brennan, I. Kovacic, On the effects of shaker dynamics on the response of a non-linear oscillator under test, *Booklet of Abstracts, EUROMECH Colloquium 503 Non-linear Normal Modes, Dimension Reduction and Localization in Vibrating Systems*, Rome, Italy, 27 September–2 October 2009, pp. 70–73.
[11] A. Carrella, M.J. Brennan, I. Kovacic, T.P. Waters, On the force transmissibility of a vibration isolator with quasi-zero stiffness, *Journal of Sound and Vibration* 322 (2009) 707–717.
[12] R.A. Ibrahim, Recent advances in nonlinear passive vibration isolators, *Journal of Sound and Vibration* 314 (2008) 371–452.
[13] J.J. Thomsen, *Vibration and Stability: Advanced Theory, Analysis, and Tools*, Springer, Berlin, 2003.
[14] A.H. Nayfeh, D.T. Mook, *Non-linear Oscillations*, second ed., Wiley, New York, 1995.